Songklanakarin J. Sci. Technol.
43 (3), 660-666, May - Jun. 2021

http://www.sjst.psu.ac.th

Original Article

Iron decorated n-TiO_2 film with enhanced photocatalytic activity under visible irradiation

Chonlada Dechakiatkrai Theerakarunwong[1*], Waraporn Chuaychai[2], and Sukon Phanichphant[3]

[1] *Chemistry Program, Department of Science, Faculty of Science and Technology, Nakhon Sawan Rajabhat University, Mueang, Nakhon Sawan, 60000 Thailand*

[2] *Biology Program, Department of Science, Faculty of Science and Technology, Nakhon Sawan Rajabhat University, Mueang, Nakhon Sawan, 60000 Thailand*

[3] *Material Science Research Center, Faculty of Science, Chiang Mai University, Mueang, Chiang Mai, 50200 Thailand*

Received: 4 December 2019; Revised: 5 April 2020; Accepted: 30April 2020

Abstract

Removal of protein from artificial and natural wastewater was performed using Fe-doped TiO_2 film under visible light in an in-house made photoreactor. The Fe(III) dopant improved TiO_2 absorption in the visible region. Fe(III) dopant at 2.5%wt. in TiO_2 gave the highest yield of protein photodegradation. Further increase in the dopant concentration decreased photoefficiency due to a higher electron-hole recombination rate and a reduced light harvesting capability. The conditions were optimal for protein remediation in an alkaline medium with 10%v/v H_2O_2. The degradation of protein started with oxidation of amino acids, which were further broken down to carbon skeletons and ammonium ions. The carbon skeletons and ammonium ions were oxidized to carbon dioxide and nitrates, respectively. The results obtained may help understand the phytotoxicity of nanomaterials interacting in the environment, prior to their use in agriculture.

Keywords: TiO_2, photocatalytic, Fe dopant, protein

1. Introduction

The rapid development of a variety of industrial technologies, the production of textiles, electronics, medicines, pharmaceuticals, foods and beverages can cause both primary and secondary water pollution. Generally, proteins used in food manufacturing are mostly from raw eggs, along with pigments and various organic substances. The proteins reduce light penetration into water, thereby decreasing water quality. Thus, there is a challenge to find effective ways to remediate organic water pollutants.

The traditional treatment technologies, such as reverse osmosis (RO), are not effective to treat complex polluted water. They are unable to remove a wide range of organic pollutants whose accumulation causes undesirable odor, color and taste. The presence of organic pollutants in water could negatively affect aquatic animals and plants, and cause major problems also to human health.

In the recent decades, nano-crystalline TiO_2 based semiconductor photocatalysis has been extensively studied due to its promise for environmental purification with high efficiency, non-toxicity, chemical stability, and at a low cost (Fu *et al.*, 2018**,** Tang, Jiang, & Liu, 2016)**.** However, TiO_2 can absorb only 2-3% of the available UV light from the solar spectrum, which limits its efficiency (Pal & Kryschi, 2016). Combining TiO_2 with a narrow band gap semiconductor has improved its visible light driven band gap level and retarded the electron/hole recombination (e^-/h^+) in practical applications. Major efforts are devoted to expand the photo-absorption of TiO_2 to longer wavelengths by doping TiO_2 with various metals (e.g. Fe^{3+}, Co^{3+}, Sn^{4+}, Mo^{5+}, Cr^{3+}) or with non-metallic elements (e.g. N^-, C^-, P^-). Numerous investigations

*Corresponding author
Email address: chonlada.dechakiatkrai@gmail.com

have reported that Fe^{3+} doping significantly improves the photo-activity of TiO_2 when introduced into the crystal lattice of TiO_2, by increasing the specific surface area of TiO_2. However, many investigations have clarified that the modified TiO_2 does not exhibit improved photocatalytic performance by itself. The effects depend on dopant concentration, catalyst content, etc (Alkaim *et al.*, 2014, Moradi, 2016, Theerakarunwong & Phanichphant, 2018).

In the present study, the degradation of protein using Fe-doped TiO_2 film was studied under visible irradiation in an in-house made photoreactor. Factors expected to affect photocatalytic efficiency were investigated, and the films were further applied to photo-decomposition of protein in contaminated wastewater under solar stimulation.

2. Experiments

2.1 Materials

The following analytical and commercial reagents were used: Titanium (IV) isopropoxide (Aldrich), iron (III) acetylacetonate (Aldrich), triton x-100 (Acros Organies), absolute ethanol (Merck), ammonia solution (Aldrich), hydrochloric acid (Aldrich), methyl red (Lobachemie), and protein standard (Aldrich). A photoreactor was self-made in the laboratory (Theerakarunwong & Phanichphant, 2018).

2.2 Photocatalyst preparation

Plain and Fe-doped TiO_2 films were synthesized and prepared as previously described (Theerakarunwong & Phanichphant, 2018). A concentration of iron (III) acetylacetonate in the range 1.0-3.0%wt. was dissolved in 20 mL of titanium (IV) isopropoxide in a cellophane membrane. Then the mixture was continuously stirred into a solution containing absolute ethanol, ammonia and deionized water at 70-80^{o}C for an hour. A powder formed during hydrolysis and condensation reactions, and was filtered with a filter paper (No.1, Whatman), washed with deionized water for 3 times, followed by vacuum drying at 110^{o}C for an hour. The white and yellow products were TiO_2 and Fe-doped TiO_2 films, respectively. In Fe-doped TiO_2 films, the amount of Fe dopant is indicated in percent by weight, at the levels 1.0, 1.5, 2.0, 2.5 and 3.0 %wt. The Fe-doped TiO_2 films were investigated.

2.3 Photocatalyst film preparation

The resultant powder from section 2.2 was dissolved in 250 mL of ethanol and mixed with deionized water at the volume ratio 1:2. Then triton x-100 was added dropwise under vigorous stirring as a binder before dip coating. A clean glass slide was mechanically dipped in the solution and subsequently calcinated at 300^{o}C for 3 h with a ramp rate of 5^{o}C/min. The not-doped and doped films were labeled with T (bare), FeT 1.0 (1.0 %Fe doped TiO_2 film), FeT 1.5 (1.5 %Fe doped TiO_2 film), FeT 2.0 (2.0 %Fe doped TiO_2 film), FeT 2.5 (2.5 %Fe doped TiO_2 film) and FeT 3.0 (3.0 %Fe doped TiO_2 film).

2.4 Characterization

The morphology and its scale in the photocatylst films were investigated using a scanning electron microscope (Fe-SEM, Jeol, JSM-6340F). The phase composition and specific surface area (SSA) were analyzed with an X-ray diffractometer (XRD) (PANalytical, X'Pert PRO) and a multi-point Brunauer, Emmett and Teller (BET) technique (Model: Autosorb 1, Quantachrome), respectively. UV-Visible spectrophotometry (UV-1280, Shimazu, Japan) was used to record the absorption spectra of all samples.

2.5 Photoactivity testing

The photocatalytic activities of the photocatalyst films were evaluated using a home-made photoreactor under visible light (Theerakarunwong & Phanichphant, 2018). Before irradiation, the suspension of protein with composite catalyst film was magnetically stirred for 30 min in dark conditions to achieve an equilibrium. Visible light illumination at 5.0 $W \cdot m^{-2}$ intensity was turned on to initiate photocatalytic reactions. During photominerization, 5 mL suspension samples were taken at 1 h intervals up to 5 h. Duplicate experiments were carried out. The contents of Fe(III), acidic/neutral/alkaline conditions, the amount of hydrogen peroxide (H_2O_2), initial concentration of synthetic wastewater and reusable water were also investigated. For protein photodegradation, the concentration of nitrate (NO_3^-), which is the expected product from photodegradation of protein, was investigated.

2.6 Toxicity evaluation

Spirodela polyrrhyza and corn were selected as model plants for water plant and terrestrial plant, respectively. Seeds of sweet corn were inoculated in autoclaved sand (10 seeds per pot, 5 pots per treatment). There were 3 treatments (distilled water, water/albumin protein without TiO_2 treatment, and water/albumin protein after TiO_2 treatment) and each treatment received different wastewater that had protein and nitrate every day (10 mL/day). After 7 days, the seedlings were removed, shoot length, root length, plant fresh weight, plant dry weight, and chlorophyll content were measured. For dry weight measurement, seedlings were dried in hot air oven at 70^{o}C for 24 h before weighing.

For *Spirodela polyrrhyza*, the plant with average fresh weight of 0.5 g was inoculated in each pot containing 50 mL water. There were 3 different treatments (7 replicates) as follows: distilled water, water/albumin protein without TiO_2 treatment, and water/albumin protein after TiO_2 treatment. After 7 days, *S. polyrrhyza* were removed and plant fresh weight, plant dry weight, and chlorophyll content were measured. Chlorophyl contents in leaves of both plant samples were analyzed and calculated using the equations available in Huang, El-Alawi, Penrose, Glick, and Greenberg (2004).

3. Results and Discussion

3.1 Characteristics of film

Fe-SEM images of FeT2.5 and FeT3.0 films are shown in Figure 1. The Fe-SEM image of FeT2.5 shows a well-defined aggregated structure, which aggregate sizes in the range 10-50 nm. TiO_2 was found to be well dispersed and fill into a pore of TiO_2 film as confirmed using XPS analysis

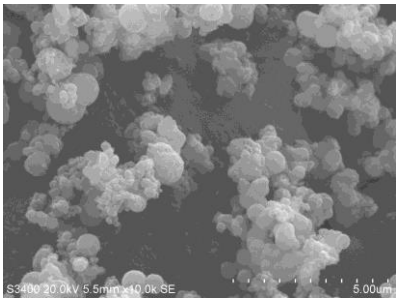

(a)

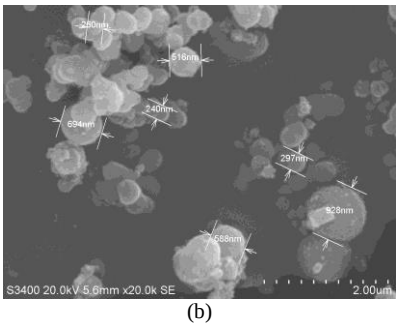

(b)

Figure 1. Fe-SEM images of (a) FeT3.0 and (b) FeT3.0 films

(Li, Shen, He, & Zu, 2008; Shehzad, Tahir, Johari, Murugesan, & Hussain, 2018; Theerakarunwong & Phanichphant, 2018). For FeT3.0 (a) and in a zoom-in of the FeT3.0 film (b), irregular structures were observed, indicating that TiO_2 was loosely embedded with Fe(III) dopant and this caused a poor interfacial connection between Ti and Fe. XRD patterns of FeT2.5 film are presented in Figure 2. A strong peak at 25θ and low intense broad peaks at 38θ, 39θ, 48θ, 54θ and 55θ firmly indicate TiO_2 anatase phase. Typical diffraction peaks of Fe-doped TiO_2 films corresponding to JCPDS file no. 78-1764 were indexed as (101) (103) (004) (112) (200) (105) (211). No Fe(III) diffraction peak was detected, which might be due to the small amount of Fe(III) dopant in the catalyst. However, according to our results published earlier, the XPS spectrum of Fe (III)-doped TiO_2 shows an extremely low content of iron in the support surface, detected in the oxide state by the XPS analysis. The observed binding energy can confirm the strong interactions between Fe and TiO_2 by the XPS peak of Fe2P and the binding energies of Fe2p3/2 and Fe2p1/2 (Theerakarunwong & Phanichphant, 2018). Moreover, it is possible that the annealing at 300°C could inhibit the layer-stack structure of TiO_2 films. Table 1 presents the SSA of all photocatalyst films according to nitrogen adsorption/desorption isotherms at 77K. The highest SSA was obtained for FeT2.5, whereas the lowest SSA was for the T film. Band gap reduction of Fe-doped TiO_2 films is illustrated in Figure 3. The band gap energy of TiO_2 with Fe doping gradually decreased due to overlapping/covalent coupling of Ti and Fe(III), which enabled excitation of electrons by visible light. The band gap energy of Fe-doped TiO_2 gives increased visible light absorption, leading to improved performance over plain TiO_2. As calculated from the UV/DRS based on Planck model using an absorption edge, in which the energy at the linear absorption coefficient, the band gap energy narrowing occurred from 3.3 eV for bare TiO_2 to 2.55 eV for FeT3.0 (Table 1). The band gap energy of

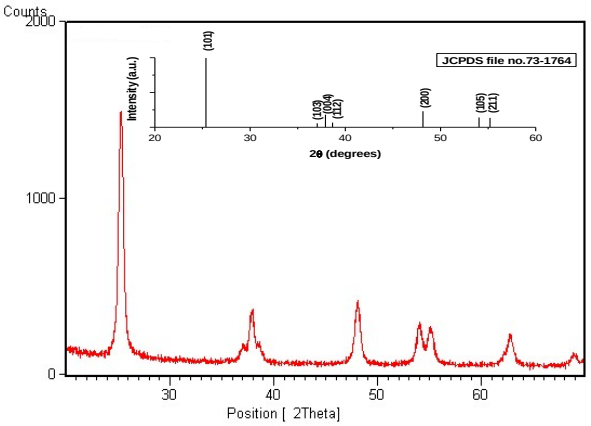

Figure 2. XRD pattern of FeT2.5 film and JCPDS file no. 78-1764 (inset)

Table 1. Characteristics of TiO_2 and Fe-doped TiO_2 films

Film	Average particle size (nm)	SSA (m^2s^{-1})	Phase	λ_{onset} (nm)	Band gap energy (eV)
T	120	68	anatase	320	3.80
FeT1.0	118	76	anatase	330	3.75
FeT1.5	111	121	anatase	335	3.70
FeT2.0	89	124	anatase	380	3.26
FeT2.5	48	159	anatase	400	3.10
FeT3.0	503	52	anatase	420	2.95

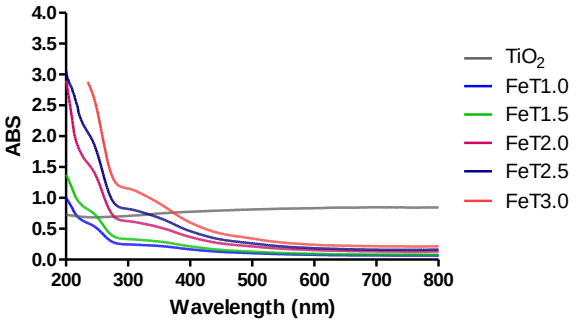

Figure 3. UV-Vis DRS spectra of TiO_2, FeT1.0, FeT1.5, FeT2.0, FeT2.5 and FeT3.0 films

Fe-doped TiO_2 films did not show significant visible narrowing. This might be because of variations in film thickness.

3.2 Effect of Fe(III) dopant dosage on photocatalytic activity

The major obstacle in TiO_2 photocatalytic oxidation of protein is the doping of Fe(III) into TiO_2 in order to enhance adsorption efficiency of visible light. Figure 4(a) illustrates the effects of Fe(III) dopant dosage on photocatalytic performance in protein degradation. The results are removal efficiencies of protein, which increased with increasing Fe(III) doping up to 2.5 %wt. and then decreased

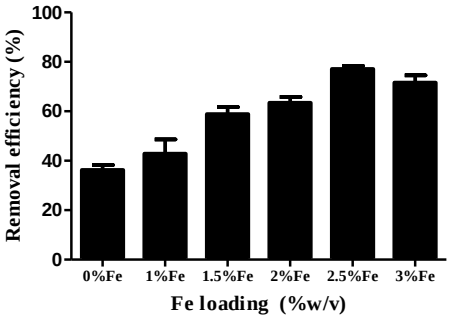

(a)

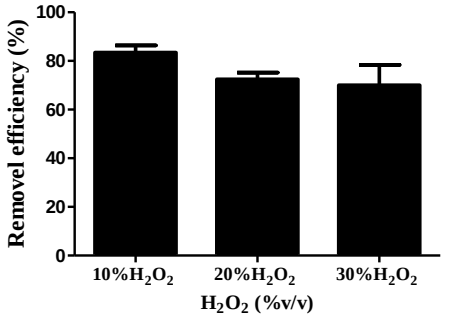

(b)

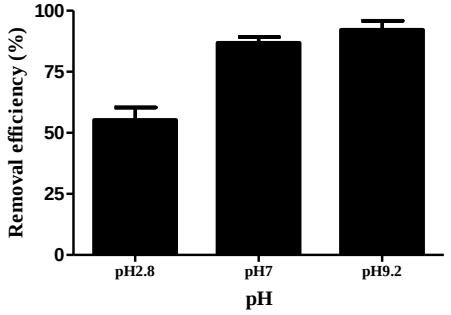

(c)

Figure 4. Protein removal efficiency from synthetic wastewater by T, FeT1.0, FeT1.5, FeT2.0, FeT2.5 and FeT3.0 films with various (a) Fe loadings, (b) $\%H_2O_2$ levels, and (c) pH levels

with further doping. The decoration of TiO_2 with Fe(III) involved photo-Fenton light catalyst, which is readily accessible for oxidation of protein molecules via $OH^{\bullet}$ produced from Fenton reaction (eq(1)-(5)) (Moradi, Eshaghi, Hosseini, & Ghani, 2016). Increasing the Fe(III) doping enhanced the activity of TiO_2 in the system, causing more $OH^{\bullet}$ oxidative species generation on the surface active sites of TiO_2. The Fe(III) concentrations exceeding 2.5%w/v reduced photocatalytic activity due to increased electron-hole recombination rate (Carević *et al.*, 2016). Although further increasing Fe continuously increased $OH^{\bullet}$ in the suspension system, the photo-efficiency decreased due to a reduced ratio of organic substance to TiO_2. Moreover, the 3.0%wt. case consistently gave a lower photodegradation activity, possibly due to the light-filtering effect, whereas concentrations of Fe(III) less than 2.5%wt. could reduce the removal efficiency of photocatalyst films due to insufficient number of $OH^{\bullet}$ radicals. The reduction of protein almost disappeared within 150 min.

$$Fe^{3+} + e^- \rightarrow Fe^{2+} \quad (1)$$
$$Fe^{2+} + h^+_{vb} \rightarrow Fe^{3+} \quad (2)$$
$$Fe^{3+} + h^+_{vb} \rightarrow Fe^{4+} \quad (3)$$
$$Fe^{4+} + e^- \rightarrow Fe^{3+} \quad (4)$$
$$Fe^{2+} + OH^{\bullet} \rightarrow Fe^{3+} + OH^- \quad (5)$$

The proposed mechanism of protein deposition involves redox reaction. Protein was oxidized firstly through visible photolysis at the peptide bonds. The cleavage of peptide was generated by cracking of carboxylic acid and ammonia. Ammonia ion (NH_4^+) was then further oxidized by $OH^{\bullet}$ radicals generated via Fe-doped TiO_2 catalyst to form NO_3^-. This could be validated by the increased NO_3^- concentration in the solution that contained protein with Fe-doped TiO_2 films. The proposed mechanism is shown in eq (6) (Naskalski & Bartosz, 2001), and Table 2 presents the concentrations of NO_3^- from various experiments.

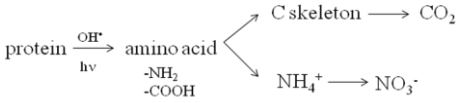

(6)

3.3 Effect of H_2O_2 on photocatalytic activity

The removal of protein was tested using different concentrations of H_2O_2. The results are shown in Figure 4(b) and Table 3. To enhance the photoactivity, H_2O_2 was added into the media to generate $OH^{\bullet}$ radicals. With 10, 20 and 30 %v/v H_2O_2, protein degradation was obviously observed at 10%v/v, at a higher rate than in the other cases. The results indicate that the efficiency of photocatalytic oxidation was accelerated by H_2O_2 which generated $OH^{\bullet}$ in the system. However, further increasing H_2O_2 concentration could decrease protein degradation efficiency. This could be attributed to inhibition of photo efficiency by a high concentration of H_2O_2, since H_2O_2 trapped $OH^{\bullet}$ radicals and led to a much weaker oxidizing $OH^{\bullet}$ radical. Moreover, $OH^{\bullet}$ radical was generated by either the direct photolysis of H_2O_2 or by the photo-oxidation of OH^- by h^+, retarding the rate of reaction (Wong & Chu, 2003, Oh *et al.*, 2016). Therefore, the optimum dosage of H_2O_2 was 10%v/v.

3.4 Effect of pH on photocatalytic activity

The photocatalytic activity of Fe-doped TiO_2 was examined by investigating the degradation of proteins under acidic (pH 2.8), neutral (pH 7.0) and alkaline (pH 9.2) conditions. The plots of pH against removal efficiency of FeT2.5 in various media are shown in Figure 4(c) and Table 4. The highest photocatalytic degradation of protein was obtained under alkaline conditions. The reason is the pH-dependent equilibrium involved NH_4^+ and NH_3 that responded by an increase in the rate of NH_4^+/NH_3 photocatalytic oxidation with increasing pH. It may be presumed that the photocatalytic oxidation to NO_3^- was limited by the electron-hole pairs formed on the surface of semiconductor by irradiation with UV-light (Alkaim *et al.*, 2014).

Table 2. Efficiency of Fe(III) dopant on protein photodegradation

Fe (III) dopant (%w/v)	Factors	
	Protein (%degradation)	NO_3^- (mM)
0	36	3.38
1.0	45	3.54
1.5	58	3.71
2.0	63	3.98
2.5	77	4.56
3.0	71	4.07

*photocatalytic activity at 150 min

Table 3. Effect of H_2O_2 on protein photodegradation

H_2O_2 (%v/v)	Photocatalytic activity at 150 min (%)
10	83
20	72
30	69

Table 4. Effect of pH of medium on protein photodegradation

pH	Photocatalytic activity at 150 min (%)
2.8	57
7.0	86
9.2	92

3.5 Effect of initial concentration of protein-contaminated synthetic wastewater

In the photocatalytic process, various concentrations of proteins (10, 20, 30, 40, 50, 60 and 70 mM) were investigated to evaluate the optimum conditions for Fe-doped TiO_2 photocatalytic activity. The maximum 93% of protein degradation was achieved when the concentration of protein was 50 mM. With further increased concentration of protein, the efficiency decreased since the increased concentration of organic substances induced an increase in organic species adsorbed by Fe-doped TiO_2 film, while the dosage of Fe(III) dopant and light intensity were constant. Moreover, the decreased amount of protein content provided insufficient amino acids or carboxylic or ammonia molecules for proteins to be adsorbed on the Fe-doped TiO_2 surfaces.

3.6 Toxicity of wastewater treated with nanocatalyst to plants

The growth of *S. polyrrhyza*, the model water plant in this experiment, varied by wastewater treatment. The wastewater treated without TiO_2 did not affected fresh weight or chlorophyll *a* content in leaves, when compared with plants grown in distilled water. Also, this water trended to increase chlorophyll *b* and total chlorophyll content compared to the plants grown in distilled water. Only plant dry weight of *S. polyrrhyza* grown in wastewater treated without TiO_2 (4.0 mg) decreased compared to the control (7.0 mg). On the other hand, the wastewater after FeT2.5 treatment tended to decrease both fresh and dry weights of *S. polyrrhyza* when compared with those grown in distilled water, and did not increase chlorophyll *b* or total chlorophyll contents from those in plants grown in wastewater without TiO_2 treatment (Figure 5(a) and Table 5).

Seeds of sweet corn, the model terrestrial plant in this experiment, could germinate and grow in sand that received wastewater at the same rate. The shoot length, plant fresh weight, plant dry weight and chlorophyll content in leaves of corn seedling that received the variously treated wastewaters did not different significantly. The shoot length in all treatments was 6.1 – 10.3 cm, while plant fresh weight and plant dry weight in all treatments were 0.52 – 0.69 g and 0.15 – 0.20 mg, respectively. However, the wastewater after FeT2.5 treatment decreased root length of corn seedlings significantly when compared to the other treatments (Figure 5(b) and Table 6). It is possible that there was some chemical only found in the wastewater after TiO_2 treatment, and this chemical inhibited the meristem at root tip that is directly exposed to wastewater in the sand. When compared with water plants exposed to wastewater, the wastewater after TiO_2 treatment also was more toxic than the others to dry weight and chlorophyll content. It is possible that some $OH^{\bullet}$ radicals from photoreactions still existed in the water and were toxic to plant growth. There is a prior report showing that some nanocomposites of Ag and Fe were toxic to *Cucumis sativus* growth, decreasing chlorophyll content and increasing oxidative stress to the plant (ChichiriccÒ & Poma, 2015, Cui, Zhang, Ma, & He, 2014).

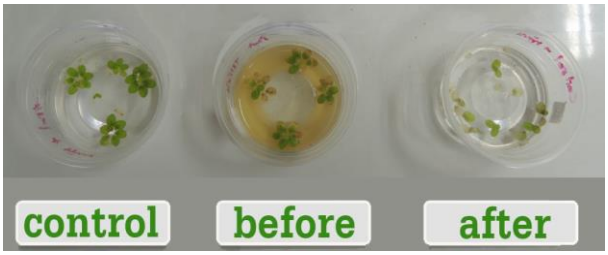

(a)

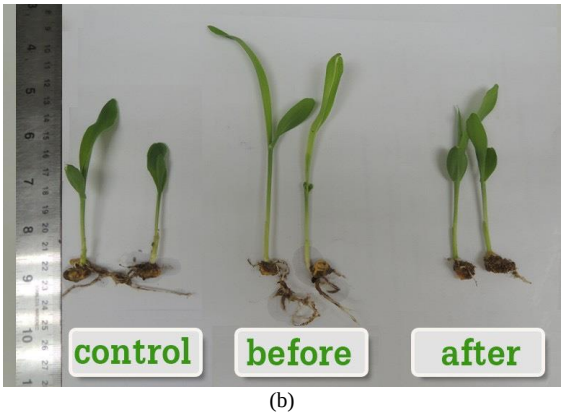

(b)

Figure 5. (a) *Spirodela polyrrhyza* grown in different wastewaters for 7 days, and (b) sweet corn seedlings grown in sand and watered with different wastewaters for 7 days; control = distilled water; before = wastewater without TiO_2 treatment; after = wastewater after TiO_2 treatment.

Table 5. Mean ± SD of *Spirodela polyrrhyza* growth when exposed to treated wastewater

Treatment	FW (g)	DW (mg)	Chlorophyll *a* (mg/ml)	Chlorophyll *b* (mg/ml)	Total chlorophyll (mg/ml)
Control	0.24 ± 0.07a	7.0 ± 1.4	1.4 ± 0.31a	0.6 ± 0.14b	2.0 ± 0.44b
Without TiO_2 treated	0.27 ± 0.07a	4.0 ± 0.4	2.3 ± 0.66a	2.5 ± 0.69a	4.8 ± 1.26a
With TiO_2 treated	0.10 ± 0.03b	3.0 ± 0.6	1.4 ± 0.10a	0.9 ± 0.05b	2.3 ± 0.06b

The data represent the mean±SD (n = 3). Different letters indicate significant differences among treatments at $p \leq 0.05$.

Table 6. Mean ± SD of corn seedling growth when exposed to treated wastewater

Treatment	Shoot length (cm)	Root length (cm)	Plant FW (g)	Plant DW (mg)	Chlorophyll *a* (mg/mL)	Chlorophyll *b* (mg/mL)	Total chlorophyll (mg/mL)
Control	6.1 ± 1.93a	5.0 ± 1.22a	0.52 ± 0.06a	0.15 ± 0.04a	9.6 ± 4.98a	3.4 ± 4.37a	13.0 ± 2.95a
Without TiO_2 treated	10.3 ± 4.36a	5.2 ± 2.32a	0.69 ± 0.16a	0.20 ± 0.05a	15.2 ± 3.67a	6.6 ± 3.13a	21.8 ± 6.20a
With TiO_2 treated	7.6 ± 1.33a	2.2 ± 0.68b	0.58 ± 0.08a	0.17 ± 0.02a	5.4 ± 6.34a	2.2 ± 1.96a	7.6 ± 6.85a

The data represent the mean±SD (n = 3). Different letters indicate significant differences among treatments at $p \leq 0.05$.

4. Conclusions

Fe-doping of TiO_2 drastically extended TiO_2 absorbance to the visible light region. The wavelength of maximum light absorbance was red-shifted. This indicates the influence of Fe(III) doping on the oxidation level of TiO_2. Fe(III) ions had a smaller band gap energy than TiO_2, hence could harvest photons within the visible region and generate electron-hole pairs. UV-Vis absorption spectra indicated that Fe affected the red shift of TiO_2 in comparison with plain TiO_2, and this was attributed to the existence of Fe(III). 2.5%wt Fe doping of TiO_2 with 10%v/v H_2O_2 loading under alkaline conditions exhibited excellent photocatalytic activity for protein degradation. No TiO_2 nanoparticles were found in the plant tissues. The low bioavailability of Ti may be due to Ti dissolution and the presence of Ti(II) or Ti(III), which have low capacities to penetrate through cell membranes. Phytotoxicity of the degraded metabolites and effluent of Fe doped TiO_2 composite after photocatalytic treatment was found. This might be due to the oxidative stress from remaining excess $OH^{\bullet}$ radicals. Further research on photocatalytic activity to degrade toxic organic substances on surface-modified catalysts will be pursued.

Acknowledgements

The authors would like to thank Faculty of Science and Technology, Nakhonsawan Rajabhat University for financial support and facilities throughout the research work.

References

Alkaim, A. F., Aljeboree, A. M., Alrazaq, N. A., Baqir, S. J., Hussein, F. H. & Lilo A. J. (2014). Effect of pH on adsorption and photocatalytic degradation. *Asian Journal of Chemistry, 26(24)*, 8445-8448. Retrieved from https://www.researchgate.net/publication/269221676.

Carević, M., Abazović, N. D., Savić, T., Novaković, T. B., Mojović, M. D. & Čomor, M. I. (2016). Structural, optical and photodegradation properties of pure and Fe-doped Titania Nanoparticles Probed using Simulated Solar Light. *Ceramics International, 42(1)B*, 1521-1529. Retrieved from https://www.sciencedirect.com/science/article/pii/S0272884215018088.

ChichiriccÒ, G. & Poma, A. (2015). Penetration and toxicity of nanomaterials in higher plants. *Nanomaterials, 5*(2), 851-873. Retrieved from https://www.ncbi.nlm.nih.gov/pubmed/28347040.

Cui, D., Zhang, P., Ma, Y. & He, X. (2014). Phytotoxicity of silver nanoparticles to cucumber (*Cucumis sativus*) and wheat (*Triticum aestivum*). *Journal of Zhejiang University - Science A: Applied Physics and Engineering, 15(8)*, 662-670. Retrieved from https://link.springer.com/article/10.1631/jzus.A1400114.

Fu, H., Yang, L., Hu, D., Yu, C., Ling, Y., Xie, Y., . . . Zhao, J. (2018). Titanium dioxide nano-heterostructure with nanoparticles decorating nanowires for high-performance photocatalysis. *International Journal of Hydrogen Energy, 43(22)*, 10359-10367. Retrieved from https://www.researchgate.net/publication/325062440.

Huang, X.-D., El-Alawi, Y., Penrose, D. M., Glick, B. R. & Greenberg, B. M. (2004). Responses of Three Grass Species to Creosote during Phytoremediation. *Environmental Pollution, 130*, 453-463. Retrieved from https://www.ncbi.nlm.nih.gov/pubmed/15182976.

Li, Z., Shen, W., He, W. & Zu, X. (2008). Effect of Fe-doped TiO_2 nanoparticle derived from modified hydrothermal process on the photocatalytic degradation performance on methylene blue. *Journal of Hazardous Materials, 15, 155(3)*, 590-4. Retrieved from https://www.sciencedirect.com/science/article/abs/pii/S0304389407017268.

Moradi, H., Eshaghi, A., Hosseini, S. R. & Ghani, K. (2016). Fabrication of Fe-doped TiO_2 nanoparticles and investigation of photocatalytic decolorization of reactive red 198 under visible light irradiation. *Ultrasonics Sonochemistry, 32*, 314-319. Retrieved from https://www.semanticscholar.org/paper/Fabrication-of-Fe-doped-TiO2-nanoparticles-and-of-Moradi-Eshaghi/b60f3c6503b9517fe29c638f3835e44ff286e26b.

Naskalski, J. W., & Bartosz, G. (2001). Oxidative modification of protein structure. *Advances in Clinical Chemistry, 35*,161-253. Retrieved from https://www.ncbi.nlm.nih.gov/pubmed/11040960

Oh, B-T, Seo, Y-S, Sudhakar, D., Choe, J-H., Lee, S-M., Park, Y-J. & Cho, M. (2016). Oxidative degradation of endotoxin by advanced oxidation process (O_3/H_2O_2 & UV/H_2O_2). *Journal of Hazardous Materials, 279*, 105–110. Retrieved from https://www.ncbi.nlm.nih.gov/pubmed/25038578.

Pal, N. B. & Kryschi, C. (2016). Improved photocatalytic activity of gold decorated differently doped TiO_2 nanoparticles: A comparative study. *Chemosphere, 144*, 1655-1664. Retrieved from https://www.sciencedirect.com/science/article/pii/S0045653515302551.

Shehzad, N., Tahir, M., Johari, K., Murugesan, T. & Hussain, M. (2018). A critical review on TiO_2 based photocatalytic CO_2 reduction system: Strategies to improve efficiency. *Journal of CO_2 Utilization, 26*, 98-122. Retrieved from https://www.sciencedirect.com/science/article/abs/pii/S2212982017307850.

Tang, R., Jiang, Q. & Liu, Y. (2016). Preparation and study on photocatalytic activity of N-doped TiO_2 decorated N-doped Graphene. *Procedia Engineering, 205*, 573–580. Retrieved from https://www.sciencedirect.com/science/article/pii/S1877705817350981.

Theerakarunwong, D. C. & Phanichphant, S. (2018). Visible-light-induced photocatalytic degradation of PAH-contaminated soil and their pathways by Fe-doped TiO_2 Nanocatalyst. *Water Air and Soil Pollution, 229(9)*. Retrieved from https://www.researchgate.net/publication/327066823.

Wong, C. C. & Chu, W. (2003). The hydrogen peroxide-assisted photocatalytic degradation of alachlor in TiO_2 suspensions. *Environmental Science and Technology, 37*, 2310-2316. Retrieved from https://pubs.acs.org/doi/10.1021/es020898n.

Zhu, X., Castleberry, S., Nanny, M. A., & Butler, E. C. (2005). Efficiency of different catalysts on removal of methylene blue. *Environmental Science and Technology, 39(10),* 3784–3791. Retrieved from https://www.researchgate.net/publication/269221676.